Simulation studies on temperature profile stiffness in ITG turbulent transport of helical plasmas for flux-matching technique

Simulation studies on temperature profile stiffness in ITG turbulent transport of helical plasmas for flux-matching technique

M. Nunami,[1,2,a)] M. Nakata,[1,2] S. Toda,[1] A. Ishizawa,[3] R. Kanno,[1,2] and H. Sugama[1,2]

[1)] *National Institute for Fusion Science / National Institutes of Natural Sciences, Toki 509-5292, Japan*

[2)] *The Graduate University for Advanced Studies, Toki 509-5292, Japan*

[3)] *Graduate School of Energy Science, Kyoto University, Uji 611-0011, Japan*

In the framework of the flux-matching method, which is a useful way for the validation of the gyrokinetic turbulence simulations, it is strongly demanded to evaluate the plasma profile sensitivity of the transport coefficients obtained in the employed simulation model within the profile gradient ranges estimated from the experimental observations. The sensitivity causes the plasma profile stiffness for wide ranges of the transport fluxes. In the nonlinear gyrokinetic simulations for the ion temperature gradient (ITG) turbulence in the Large Helical Device (LHD) [Y. Takeiri, *et al.*, Nucl. Fusion **57**, 102023 (2017)], it is found that the temperature gradients around the experimental nominal observations are slightly larger than the threshold of the instability, and the ion heat diffusivities are quite sensitive to the temperature gradient. The growth rates of the instability, the generations of the zonal flows, and the sensitivities of the transport coefficients to the temperature profiles depend on the radial locations, the employed simulation models, and the field configurations. Especially, in the optimized LHD field configuration, the sensitivities are relaxed in outer radial region due to the enhancement of the zonal flows and the reduction of the ITG instability. In order to estimate the range of the temperature gradients possible given the experimentally obtained data of the temperature with errorbars, the statistical technique, Akaike's Information Criterion [H. Akaike, Proceedings of the 2nd International Symposium on Information Theory, 267 (1973)] is applied. Against the range of the temperature gradients, the flux-matching method to predict the temperature gradient in helical plasmas are demonstrated.

Keywords: Turbulent transport, Profile stiffness, Akaike's Information Criterion, Large Helical Device

[a)] nunami.masanori@nifs.ac.jp

I. INTRODUCTION

Understanding of the plasma turbulent transport phenomena has been regarded as one of the most critical issues in the magnetically confined plasmas research. The gyrokinetic approaches[1] are powerful for analyzing the turbulent transport, which are considered to be driven by the drift-wave plasma turbulence. The turbulent transport fluxes obtained in the gyrokinetic simulations are quite sensitive to the profiles of the radial gradients of the plasma temperature and density, which concludes the stiffness of the plasma profiles. In the gyrokinetic simulations in DIII-D tokamak L-mode plasma in outer radial region, a significant underprediction of the ion heat transport, namely, the transport shortfall, has been reported.[2,3] In the past few years, there has been discussion that the transport shortfall might be caused by shortcomings of the gyrokinetic theory or missing physics in the numerical gyrokinetic codes. However, the simulations by GENE code indicated that the transport shortfall is much less pronounced and can be removed by mild changes of the ion temperature profile[4] because of the strong stiffness of the ion temperature profiles against the ion heat transport fluxes. In addition to the plasma profile ambiguities, the uncertainty quantification of the simulation results for the transport fluxes is also significant for the validation studies.[5] One of useful validation ways of the turbulence simulations is the flux-matching method, in which the temperature and density gradients are determined so as to match the transport fluxes from the simulations with the experiments, based on the sensitivities of the transport fluxes to the profile gradients of the plasmas. Therefore, as far as the simulations or models for the turbulent transport are employed, the precise estimates of the plasma profile sensitivity of the transport in the employed simulation models within the experimentally allowable ranges of the plasma profile gradients, i.e. the ranges of the profile gradients possible given the experimentally obtained data of the plasma profiles with errorbars, should be regarded as one of the most significant issues in terms of a concrete way for the validation metrics[6] of the simulations and models.

In the stellarator systems, on the other hand, while there are several important gyrokinetic simulation studies on the turbulent transport[7–9], there are not many studies on the plasma profile sensitivities to validate the simulation results against the specific experimental results. In the linear stability analyses[10] for the high ion temperature plasmas in the Large Helical Device (LHD)[11], the ion temperature gradient (ITG) modes are unstable at

the temperature gradients around the experimental nominal observations. The ion temperature gradients around the experimental observations in the plasma are slightly higher than the threshold of the instability, beyond which the linear growth rates rapidly grows. In this paper, we focus on the high ion temperature LHD plasmas where the ITG modes are dominant instability. By means of the gyrokinetic simulations, we evaluate the sensitivities of the turbulent ion heat diffusivities to the temperature gradients in the LHD plasma. Based on the statistical treatment for the experimental errorbars of the temperature, the Akaike's Information Criterion (AIC)[12,13], the experimentally allowable ranges of the temperature gradients are determined. Using the simulation results of the profile sensitivity in the turbulent transport, we demonstrate the flux-matching method to predict the temperature gradients which are compared with the statistically inferred allowable temperature gradient ranges from the LHD experiment.

This paper is organized as follows. In Sec. II, we briefly describe the simulation model used in the present study and basic equations employed in the calculation. In Sec. III, the linear instability in high-$T_{\rm i}$ LHD plasma is briefly reviewed and the nonlinear simulation results for the sensitivities to the plasma temperature gradients in the turbulent transport are shown. In Sec. IV, the radial ion temperature profiles are statistically inferred from the experimental observations to specify the allowable temperature gradient ranges, and the flux-matching method is demonstrated to validate the simulation results. Finally, a summary is given in Sec. V.

II. GYROKINETIC SIMULATION MODEL

In this paper, in order to evaluate the turbulent transport of the helical plasmas, we employ the local δf flux-tube gyrokinetic code, GKV.[14,15] The code can solve the time evolution of the wavenumber-space representation of the gyrokinetic equation for the perturbed gyrocenter distribution function of species s in the three-dimensional equilibrium field. The perturbed distribution function is represented by $\delta f_{sk_\perp} = -e_s J_{0s} \delta\phi_{k_\perp} F_{{\rm M}s}/T_s + h_{sk_\perp}$, where $h_{sk_\perp}$ is the non-adiabatic part of the perturbed distribution function. The gyrokinetic equation for $h_{sk_\perp}$ is

$$\left(\frac{\partial}{\partial t} + v_\parallel \boldsymbol{b}\cdot\nabla + i\omega_{{\rm D}s} - \frac{\mu \boldsymbol{b}\cdot\nabla B}{m_s}\frac{\partial}{\partial v_\parallel} \right) h_{sk_\perp}$$

$$-\frac{c}{B}\sum_{\Delta}\boldsymbol{b}\cdot(\boldsymbol{k}'_{\perp}\times\boldsymbol{k}''_{\perp})\delta\Psi_{k'_{\perp}}h_{sk''_{\perp}}$$
$$=\frac{e_sF_{\mathrm{M}s}}{T_s}\left(\frac{\partial}{\partial t}+i\omega_{*Ts}\right)\delta\Psi_{k_\perp}+C_s(h_{sk_\perp}), \tag{1}$$

where e_s, T_s, and m_s are the electric charge, the equilibrium temperature, and the particle mass of the species s, respectively. The magnetic moment $\mu = v_\perp^2/2B$ and the parallel velocity $v_\parallel$ are employed as the velocity space coordinates. $\delta\Psi_{k_\perp} = J_{0s}[\delta\phi_{k_\perp} - (v_\parallel/c)\delta A_{\parallel k_\perp}]$ is the gyro-averaged potential fluctuation with the zeroth order Bessel function $J_{0s} = J_0(k_\perp v_\perp/\Omega_s)$ and $\Omega_s = e_sB/(m_sc)$ is the gyrofrequency of the particle species s. And $\omega_{\mathrm{D}s} = \boldsymbol{k}_\perp\cdot\boldsymbol{v}_{s\mathrm{D}}$ and $\omega_{*Ts} = \boldsymbol{k}_\perp\cdot\boldsymbol{v}_{s*}$ are the magnetic and the diamagnetic drift frequencies with $\boldsymbol{v}_{s\mathrm{D}} = (c/e_sB)\boldsymbol{b}\times(\mu\nabla B + m_sv_\parallel^2\boldsymbol{b}\cdot\nabla\boldsymbol{b})$ and $\boldsymbol{v}_{s*} = (cT_s/e_sB)\boldsymbol{b}\times[\nabla\ln n_s + (m_sv^2/2T_s - 3/2)\nabla\ln T_s]$, respectively. A linearized model collision operator C_s is introduced using a simplified Lenard-Bernstein model for the numerical scans for wide-parameter regimes. In Eq.(1), the symbol $\sum_\Delta$ represents double summations with respect to $\boldsymbol{k}'_\perp$ and $\boldsymbol{k}''_\perp$, satisfying $\boldsymbol{k}_\perp = \boldsymbol{k}'_\perp + \boldsymbol{k}''_\perp$, and the equation is solved in the local flux-tube coordinates, $\{x, y, z\} = \{a(\rho-\rho_0), a\rho_0q(\rho_0)^{-1}[q(\rho)-\zeta], \theta\}$ with conventional flux-coordinate system $\{\rho, \theta, \zeta\}$. Here, a is the minor radius, and $q(\rho_0)$ is the safety factor at the focused magnetic flux surface labeled by ρ_0, and $\rho \equiv \sqrt{\psi/\psi_{\mathrm{a}}}$ is the normalized radial coordinate. Here ψ represents the toroidal magnetic flux, and ψ_{a} is also defined by the value at the last closed surface. The fluctuations of the potentials are calculated by the Poisson and Ampère equations,

$$\left(k_\perp^2 + \lambda_{\mathrm{D}}^{-2}\right)\delta\phi_{k_\perp} = 4\pi\sum_s e_s\int d\boldsymbol{v}J_{0s}h_{sk_\perp}, \tag{2}$$
$$k_\perp^2\delta A_{\parallel k_\perp} = \frac{4\pi}{c}\sum_s e_s\int d\boldsymbol{v}v_\parallel J_{0s}h_{sk_\perp}. \tag{3}$$

Here, λ_{D} is the Debye length.

III. SENSITIVITY TO THE TEMPERATURE GRADIENTS

In high-T_{i} LHD plasma experiment #88343[16,17], gyrokinetic analyses with kinetic electrons[18] and adiabatic electrons[10,19] were performed and the linear analyses of the micro-instabilities were also evaluated precisely. In order to grasp the properties of the instabilities and the turbulent transport in the plasma, we discuss both results obtained from the simulation models with kinetic and adiabatic electrons.

A. Microinstability in high-T_i LHD plasma

In our papers[10,18,19], as shown in Fig.1(a), the poloidal wavenumber spectra of linear growth rates and real frequencies of the micro-instabilities at $\rho = 0.65$ in the LHD high-T_i plasma were obtained from electromagnetic simulations with kinetic electrons and the electrostatic simulations with adiabatic electrons. In this plasma, we found that the ITG modes with negative real frequency, which means mode propagation in the direction of ion diamagnetic rotation in the GKV code, are most unstable. As seen in the figure, the growth rates in the kinetic electron case are about two times larger than that of the adiabatic electron calculation where the kinetic electrons cause the enhancement of the ITG mode.[18] In order to evaluate the plasma profile dependences of the instability, we plot the dependences of the maximum growth rates γ_max of the micro-instability on the normalized ion temperature gradients $R_0/L_{T\mathrm{i}}$ in Fig.1(b). Here, $L_{T\mathrm{i}}$ is the ion temperature gradient scale length defined by $L_{T\mathrm{i}} \equiv -\mathrm{d}\ln T_\mathrm{i}/dr$, and R_0 is the major radius of the magnetic axis. While both results have strong sensitivities in the kinetic and adiabatic electron cases, we calculate the critical values of $R_0/L_{T\mathrm{i}}$ for the threshold of the linear instability as shown in Fig.3. Because of the enhancement of the growth rates in the kinetic electron case as shown in Fig.1(a), there are clear differences between both cases for not only the dependences of the growth rates but also the linear critical gradient. That is, the critical gradient in the kinetic electron case is changed to be smaller than the adiabatic electron calculations.

B. Turbulent transport coefficients

In order to analyze the sensitivity of the turbulent transport to the temperature gradients in helical plasmas, we perform the nonlinear gyrokinetic simulations with kinetic and adiabatic electrons for the ITG turbulent transport by using GKV code. In the simulations, we employ the same plasma profiles and the field configurations for LHD discharge #88343 used in the previous papers.[18,27] Figure 2 shows the heat diffusivities obtained by the ITG turbulence simulations changing the normalized ion temperature gradients $R_0/L_{T\mathrm{i}}$. If we use the fitting function of $\chi/\chi_\mathrm{i}^\mathrm{GB} = A_0(1 - A_1/(R_0/L_{T\mathrm{i}}))$ which is employed in Dimits's papers[20,21] to the simulation results, where A_0 and A_1 are the fitting coefficients, we can obtain the nonlinear critical temperature gradients for the cases of the kinetic electron and

the adiabatic electron calculations as shown in Fig.3. Here, $\chi_{\rm i}^{\rm GB} \equiv \rho_{\rm ti}^2 v_{\rm ti}/R_0$ with the ion thermal gyroradius $\rho_{\rm ti} \equiv v_{\rm ti}/(eB_0/m_{\rm i}c)$ and the ion thermal speed $v_{\rm ti} = \sqrt{T_{\rm i}/m_{\rm i}}$ are defined. In Figs.2 and 3, it is found that the sensitivity of the ion heat diffusivity to the temperature gradients in the kinetic electron calculation case is steeper and the critical temperature gradient is smaller than the adiabatic electron case. These results are similar to the linear analyses in the previous section. We also find that there are up-shifts of the nonlinear critical temperature gradients $R_0/L_{T\rm i}^{\rm (NL.crit.)}$ from linear critical values $R_0/L_{T\rm i}^{\rm (Lin.crit.)}$, e.g., the Dimits shift. The widths of the up-shifts $\Delta^{\rm (Shift)} \equiv R_0/L_{T\rm i}^{\rm (NL.crit.)} - R_0/L_{T\rm i}^{\rm (Lin.crit.)}$ for both cases are

$$\begin{array}{ll} \Delta^{\rm (Shift)} = 0.606 & \text{(w/ kinetic electrons)} \\ \Delta^{\rm (Shift)} = 1.136 & \text{(w/ adiabatic electrons)} \end{array}, \tag{4}$$

the width in the case of kinetic electron calculation is narrower than in the case of adiabatic electrons. Of course, the fitting procedures to obtain the relation between $\chi_{\rm i}$ and $R_0/L_{T\rm i}$ have still ambiguities due to the numerical and statistical uncertainties of the simulation results.[5] Therefore, the widths of the up-shifts can be slightly changed within the uncertainties, although it can remain that the up-shifts width with kinetic electrons is narrower than the width with adiabatic electrons.

The micro-instabilities are affected by the magnetic field geometry such as the magnetic shear and the curvature. The growth rates of the instabilities are reduced for small safety factor and strong negative shear due to the reduction of the bad curvature region as shown in Ref.[22] Indeed, Fig.5(a) shows that the safety factor q and the magnetic shear $\hat{s} \equiv (\rho/q)dq/d\rho$ in the LHD case radially change. Therefore, the radial properties for the temperature gradient dependences of the turbulent transport are also significant in the helical plasma transport phenomena. In order to evaluate the changes of the dependences along the radial direction, we must perform more nonlinear gyrokinetic simulations at several flux-surfaces. Therefore, we discuss here only the adiabatic electron cases, since the simulations with kinetic electrons in helical plasmas cannot be performed for several radial locations because of its computationally quite expensive costs. We perform the simulations with adiabatic electrons at radial positions between $\rho = 0.46$ to 0.83 in the LHD plasma. From the results, at least in the adiabatic electron simulations, we can evaluate the critical temperature gradients for a wide range of the radial direction and their up-shift widths from linear critical values. In Fig.3, the width of the up-shift have radial dependencies, that is, the width tends to become large for middle radial regions, $0.5 < \rho < 0.7$. Furthermore, the critical gradient

is more exceeded the experiment for the outer radial region than the inner region. This means that the instabilities are more marginal for inner radial region in the LHD plasma.

C. Optimized field configuration

In helical systems, the magnetic field configuration with the inward shifted magnetic axis is one of the neoclassical transport optimized configurations.[23] In the optimized case, the radial drift velocity of helically trapped particles is reduced, and the zonal flow response becomes more favorable because the shielding effect of the helically trapped particles is weakened.[24] Therefore, in the configuration, the turbulent transport is also reduced because of the greater enhancement of zonal flow generations.[9,25,26] In the present section, within the simulations with the adiabatic electrons, we evaluate the sensitivity of the ion heat turbulent transport coefficients to the ion temperature gradients in two cases of the LHD field configurations, that is, the optimized LHD configuration with the inward shifted magnetic axis and the standard LHD configuration which is same configuration discussed in the previous section. Figure 4 shows the ion temperature gradient dependencies of the ion heat transport coefficients by the simulations with adiabatic electrons. Here, the simulations in the inward shifted case are performed with the same plasma profiles of the standard case except for the field configuration. While the sensitivities depend on the radial location in both configurations, the transport coefficients in outer radial region are reduced and the sensitivity to the temperature gradients are more relaxed in the optimized configuration than the cases of the standard configuration. On the other hand, in inner radial region, the sensitivity cannot be changed in both configurations. Therefore, in the optimized LHD configuration, higher confinement performances are realized for outer radial region, because the relaxed sensitivity to the temperature gradient means that we can reach higher temperature with the same input power into the plasma.

Based on the relation between the linear stability analyses and the nonlinear turbulence simulations, where the concepts of the relation are explained in our previous work[27], we can estimate the summation of the linear growth rates divided by square of wavenumber $\sum_{ky}(\gamma/k_y^2)$ regarded as the nonlinear turbulence component, and the zonal flow decay time $\tau_{\rm ZF} = \int dt \langle\phi(t)\rangle / \langle\phi(0)\rangle)$ regarded as the ratio of the nonlinear zonal flow component and the turbulence component. Here, $\phi(t)$ is the linear response function of the zonal flow

potentials. In Fig. 5, we plot the radial profiles of the linear growth rates $\sum_{ky}(\gamma/k_y^2)$, the zonal flow decay time $\tau_{\rm ZF}$, the normalized ion heat transport coefficients $\chi_{\rm i}/\chi_{\rm i}^{\rm GB}$, and the nonlinear critical temperature gradients $R_0/L_{T{\rm i}}^{\rm (NL.crit.)}$ in both field configurations. While the linear growth rates in the optimized configuration are larger than that of the standard configuration in the inner radial region, the growth rates in the outer region becomes small in the optimized configuration compared with the standard case. The zonal flow decay time in the optimized configuration remains larger than the standard case. Therefore, in the outer radial region for the optimized configuration, the transport reduction effects by the zonal flows are enhanced, and the resultant transport coefficients and the sensitivities to the temperature gradients are strongly reduced compared with the standard configuration. For the nonlinear critical temperature gradients, on the other hand, even though the relaxed sensitivity and the enhancement of zonal flow generation are clearly found in the outer radial region for the optimized field configuration case, the critical values are little changed from the standard case as shown in Fig.5(d). However, the up-shift width of the nonlinear critical temperature gradients from linear critical values in the optimized configuration case is

$$\Delta^{\rm (Shift)} = 1.616 \ \ \text{(for optimized config.)}, \tag{5}$$

at $\rho = 0.65$. At least in the simulations with adiabatic electrons, the width is clearly enhanced compared with the standard configuration case in Eq.(4) for the adiabatic electron case, $\Delta^{\rm (Shift)} = 1.136$, due to the the enhancement of the zonal flows and the reduction of the turbulent transport as shown in Fig.5.

IV. TRANSPORT COEFFICIENTS AGAINST EXPERIMENT

As shown in the previous sections for the turbulent transport simulation studies, it is quite significant to determine the temperature gradients from the experimental observations as an input of the instability sources. As a context for the validation of the gyrokinetic simulations, in the recent works[28,29] the statistical approach of the profile fitting to the discrete experimental data using a non-parametric regression technique based on the Gaussian process regression[30] has been employed for the uncertainty in the experimental measurements. In the present section, we employ a different statistical technique for the profile fitting analyses, the Akaike's Information Criterion (AIC)[12,13], because the technique enables us to

obtain the probable function forms of the temperature profiles statistically inferred from the experiments, and the technique is one of the useful measures for the relative quality of the fitting functions based on the maximum likelihood principle. The temperature profiles including the error ranges can be obtained from the fitting technique based on the AIC technique. Using the forms of the temperature profiles, the experimentally allowable ranges of the temperature gradient profiles are obtained, and we estimate the ranges of the ITG turbulent transport coefficients within the experimentally allowable ranges of the temperature gradients. Using the results for the temperature gradient sensitivities of the turbulent transport discussed in the previous section and the experimentally allowable range of the temperature gradient profiles, the radial temperature gradients profiles are expected in terms of the flux-matching method.

A. Temperature gradient within experimental errors

In the LHD experiments, the plasma temperatures are measured by the charge exchange recombination spectroscopy (CXRS), and the obtained data have the precise errorbars at each radial position. When we have only discrete data of the plasma temperatures with such errorbars, we must extract the radial gradient of the temperature from the data, because we have no direct measurements of the temperature gradients. In terms of general statistics, the widths of the errorbars are regarded as the standard deviation of the measurement data. Therefore, we can reproduce the temperature data by generating the normal distributions $\mathcal{N}(T(\rho_i), \sigma^2(\rho_i))$ with the average $T(\rho_i)$ and the standard deviations $\sigma(\rho_i)$ which correspond to the errorbars at each radial position ρ_i. Here, we focus on the ion temperature data obtained in the LHD high-$T_{\rm i}$ experiment #88343.[16,17] After the normal distributions at each radial position are reproduced from the experimental data, we choose the combinations of the temperature data of the reproduced distributions at each radial position by random sampling. For each combination, we obtain the fitting functions with a certain function form of the normalized radial coordinate, $\rho \equiv \sqrt{\psi/\psi_{\rm a}}$. For simplicity, if we assume the form as the conventional power series of ψ,

$$T(\rho) = \sum_{k=0}^{N} a_k \psi^k(\rho) = \sum_{k=0}^{N} b_k \rho^{2k}, \tag{6}$$

we can obtain the radial functions of the ion temperatures corresponding to the sampling combinations of the temperature data. In the function, a_k or b_k are k-th order fitting coefficients and N is the upper bound of the order of the expansion series. For the statistical validity of the fitting, we should ask which N is the best order. In order to determine the best order of the fitting function, the AIC is employed as an indicator to obtain it. In the AIC theory based on the maximum likelihood principle, we should optimize the fitting function by minimizing a variable AIC, which is defined by

$$AIC \equiv n \log \left[\sum_{i=1}^{n} w(\rho_i) \left(t_i - T(\rho_i) \right)^2 \right] + 2N, \tag{7}$$

and the optimized best order N can be determined. Here n is the number of the discrete data points of the reproduced temperature data t_i at the radial position ρ_i for $i = 1, 2, \cdots, n$, and $w(\rho_i) \geq 0$ is the weight function at ρ_i. Since the normal distributions $\mathcal{N}(T(\rho_i), \sigma^2(\rho_i))$ at each radial position are independently generated from each experimental errorbar, we should employ the weight function of $w(\rho_i) = 1$, exactly. In this method, we have different functions with different N for each sampling combination because N can change depending on the sampling combinations. Figure 6 shows the results of the fittings with the AIC operations. By taking the radial derivatives of obtained each function, we can obtain the possible temperature gradient profiles with the certain ranges according to the experimental errors. Figure 7 shows the results of the temperature gradient profiles with the ranges from $10,000$ sampling functions in Fig. 6. In the figure, there exists some knuckle-like points which are caused by the concrete forms of each fitting function. The relative error level is large in the inner radial region, and becomes small in the outer region, while the error levels do not exceed 20 % of the medians.

B. Ranges of transport coefficients

Within the ranges of the temperature gradients obtained in the previous section, the ranges of the ion heat diffusivities for the high-$T_{\rm i}$ LHD plasma are evaluated based on the temperature gradient sensitivities of the transport coefficients in Sec.III. In the results shown in Fig. 8, the ion heat diffusivities have certain ranges because the errors of the temperature gradients estimated by AIC technique enhance the ranges of the simulation results. In the plots, the simulation result in the kinetic electron case is a little overestimated against the

experiment. On the other hand, the result in the adiabatic electron case, which does not include physics of kinetic electrons, seems to cover the experimental diffusivities. However, both results of the kinetic and the adiabatic electron simulations may cover the experimental diffusivity if we change the temperature gradient by $\pm 20\%$ as discussed in our previous paper.[18] Since there are ambiguities of the allowable ranges, which depends on the choice of the fitting function of the temperature profile and the kinds of information criterion for the maximum likelihood, the results in the plots should be regarded as the reference of the simulation models employed here.

C. Flux-matching for expectation of temperature gradients

If the heat fluxes are fixed to match the experimental observations of the transport fluxes, the temperature gradients can be expected by using the flux-matching method.[4] Since we already have the temperature gradient dependencies of the ion heat transport coefficients in Figs. 2 and 4, we can evaluate the temperature gradients which correspond to the gradients realizing the experimental transport fluxes of the ion heat. The matched temperature gradients can be regarded as the expectations of the ion temperature gradients at least in the simulation models performed here. Therefore, we perform the flux-matching for the ion temperature gradient from the simulation results, as the first reference of the expectation in helical plasmas. In Fig. 9, the results of the expectations for the LHD high-$T_{\rm i}$ plasma are shown. The results in the adiabatic electron cases seem to be close to the allowable ranges of the temperature gradients within the experimental errorbars, and the result in the kinetic electron case is underestimated compared with the adiabatic electron case. However, as discussed in Fig.8, the expectations using the simulations with kinetic electrons cover the ranges within $\pm 20\%$ of $R_0/L_{T\rm i}$. The agreements with the allowable gradient ranges for the adiabatic electron cases shown in Figs.8 and 9 should be recognized to be one of the open issues because the simulations do not include more physics compared with the kinetic electron simulations. Therefore, we should regard this result as just reference of the applications of the flux-matching method, and we must perform the matching method based on more precise electromagnetic simulations with the kinetic electrons including the unintroduced physics.

V. SUMMARY

In this paper, based on the gyrokinetic ITG turbulent transport simulations, we have evaluated the plasma profile sensitivity of the turbulent transport in the helical systems within the temperature gradient ranges estimated from the experiments. It has been found that the sensitivity to the temperature profiles depend on the radial locations, the field configurations, and the employed simulation models. Especially, for outer radial region in the optimized LHD field configuration with the inward-shifted magnetic axis, the sensitivities are clearly relaxed while the critical temperature gradients for the nonlinear turbulent transport do not change from the standard field configuration case. Due to the zonal flow enhancement and the reduction of the ITG instability in the optimized configuration, the up-shift width of the critical gradient from the linear critical value is enhanced compared with the standard configuration case. Based on these studies on the profile sensitivity, we have evaluated the turbulent transport coefficients within the ranges of the temperature gradients estimated from experimental observations. Furthermore, the flux-matching method have been demonstrated for the high-T_i LHD plasma as the first reference of the applications of the method to validate the gyrokinetic simulation models with kinetic and adiabatic electrons. The results in the adiabatic electron cases show better agreements with the allowable temperature gradient ranges than the kinetic electron case, although the adiabatic electron model is less precise than the kinetic electron model. Incidentally, in the our work[18], the electron heat diffusivity χ_e in the kinetic electron case is predicted near the experimental nominal value. However, since both gyrokinetic models and analyses employed in this paper are restricted to the ion transport simulations under the assumptions that there are still unintroduced effects, e.g., $\boldsymbol{E} \times \boldsymbol{B}$ shearing effects, which may improve the predictions for ion heat transport, we should improve the simulation model. Of course, in order to complete the flux-matching studies in the turbulence simulations, we should also discuss the electron temperature gradients and the density gradients which have significant impacts on the helical plasma turbulent transport.

In this work, the useful measure for the relative quality of the fitting functions, AIC, is employed for the evaluations of experimentally allowable range of the ion temperature gradients. However, the allowable ranges may depend on the kinds of the quality measure of the statistical models and the characteristics of the experimental data, and there are

other statistical approaches, e.g., the WAIC[31] and the Gaussian process regression. Further studies regarding these issues will appear elsewhere.

ACKNOWLEDGMENTS

The authors would like to thank Prof. K. Ida for useful discussions about CXRS measurements, and thank the LHD experiment group. This work is supported in part by the Japanese Ministry of Education, Culture, Sports, Science and Technology, Grant (Nos. 26820398, 16K06941, 17K14899, and 18H01202), by National Institute for Fusion Science (NIFS) Collaborative Research Program (KNTT043, KNTT045 and KNST095), and by the FLAGSHIP2020, MEXT within the priority study 6. The results is obtained by using the K computer at the RIKEN Advanced Institute for Computational Science (Proposal number: hp120138, hp170260, hp180200, and hp180083), Helios system at International Fusion Energy Research Center (Project code: GKMLDST, GKVPP, VLDGK, VLDGK_ST, and GTNAXIS), and "Plasma Simulator" of NIFS.

REFERENCES

[1]X. Garbet, Y. Idomura, L. Villard, and T.H. Watanabe, Nucl. Fusion **50**, 043002 (2010).

[2]C. Holland, A. E. White, G. R. McKee, M. W. Shafer, J. Candy, R. E. Waltz, L. Schmitz, and G. R. Tynan, Phys. Plasmas **16**, 052301 (2009).

[3]T.L. Rhodes, C. Holland, S.P. Smith, A.E. White, K.H. Burrell, J. Candy, J.C. DeBoo, E.J. Doyle, J.C. Hillesheim, J.E. Kinsey, G.R. McKee, D. Mikkelsen, W.A. Peebles, C.C. Petty, R. Prater, S. Parker, Y. Chen, L. Schmitz, G.M. Staebler, R.E. Waltz, G. Wang, Z. Yan, and L. Zeng, Nucl. Fusion **51**, 063022 (2011).

[4]T. Görler, A. E. White, D. Told, F. Jenko, C. Holland, and T. L. Rhodes, Phys. Plasmas **21**, 122307 (2014).

[5]P. Vaezi and C. Holland, Fusion Sci. Tech. 10.1080/15361055.2017.1372987 (2018).

[6]C. Holland, Phys. Plasmas **23**, 060901 (2016).

[7]P. Xanthopoulos, G.G. Plunk, A. Zocco, and, P. Helander, Phys. Rev. X **6**, 021033 (2016).

[8]P. Xanthopoulos, F. Merz, T. Görler, and F. Jenko, Phys. Rev. Lett. **99**, 035002 (2007).

[9]T.-H. Watanabe, H. Sugama, and S. Ferrando-Margalet, Phys. Rev. Lett. **100**, 195002 (2008).

[10]M. Nunami, T.-H. Watanabe, H. Sugama and K. Tanaka, Plasma Fusion Res. **6**, 1403001 (2011).

[11]Y. Takeiri, T. Morisaki, M. Osakabe, M. Yokoyama, S. Sakakibara, H. Takahashi, Y. Nakamura, T. Oishi, G. Motojima, S. Murakami, *et al.*, Nucl. Fusion **57**, 102023 (2017).

[12]H. Akaike, Proceedings of the 2nd International Symposium on Information Theory, Petrov, B. N., and Caski, F. (eds.), Akadimiai Kiado, Budapest: 267-281 (1973).

[13]S. Konishi and G. Kitagawa, *Information Criteria and Statistical Modeling* (Springer-Verlag New York) (2008).

[14]T.-H. Watanabe and H. Sugama, Nucl. Fusion **46**, 24 (2006).

[15]M. Nunami, T.-H. Watanabe, and H. Sugama, Plasma Fusion Res. **5**, 016 (2010).

[16]K. Tanaka, C. A. Michael, L. N. Vyacheslavov, A. L. Sanin, K. Kawahata, T. Akiyama, T. Tokuzawa and S. Okajima Rev. Sci. Instrum. **79**, 10E702 (2008).

[17]K. Tanaka, C. Michael, L. Vyacheslavov, H. Funaba, M. Yokoyama, K. Ida, M. Yoshinuma, K. Nagaoka, S. Murakami, A. Wakasa, T. Ido, A. Shimizu, M. Nishiura, Y. Takeiri, O. Kaneko, K. Tsumori, K. Ikeda, M. Osakabe, K. Kawahata and LHD Experiment Group, Plasma Fusion Res. **5**, S2053 (2010).

[18]A. Ishizawa, T.-H. Watanabe, H. Sugama, M. Nunami, K. Tanaka, S. Maeyama and N. Nakajima, Nucl. Fusion **55**, 043024 (2015).

[19]M. Nunami, T.-H. Watanabe, H. Sugama, and K. Tanaka, Phys. Plasmas **19**, 042504 (2012).

[20]A.M. Dimits, G. Bateman, M.A. Beer, B.I. Cohen, W. Dorland, G.W. Hammett, C. Kim, J.E. Kinsey, M. Kotschenreuther, A.H. Kritz, L.L. Lao, J. Mandrekas, W.M. Nevins, S.E. Parker, A.J. Redd, D.E. Shumaker, R. Sydora and J. Weiland, Phys. Plasmas **7**, 969 (2000).

[21]A.M. Dimits, B.I. Cohen, N. Mattor, W.M. Nevins, D.E. Shumaker, S.E.=Parker, and C. Kim, Nucl. Fusion **40**, No. 3Y (2000).

[22]T. Kuroda, H. Sugama, R. Kanno, and M. Okamoto, J. Phys. Soc. Jpn **69**, 2485 (2000).

[23]S. Murakami, A. Wakasa, H. Maaßberg, C.D. Beidler, H. Yamada, K.Y. Watanabe and LHD Experimental Group, Nucl. Fusion **42**, L19 (2002).

[24]S. Ferrando-Margalet, H. Sugama, and T.-H. Watanabe, Phys. Plasmas **14**, 122505 (2007).

[25]H. Sugama, and T.-H. Watanabe, Phys. Rev. Lett. **94**, 115001 (2005).

[26]H. Sugama, and T.-H. Watanabe, Phys. Plasma **13**, 012501 (2006).

[27]M. Nunami, T.-H. Watanabe, and H. Sugama, Phys. Plasmas **20**, 092307 (2013).

[28]M.A. Chilenski, M. Greenwald, Y. Marzouk, N.T. Howard, A.E. White, J.E. Rice, and J.R. Walk, Nucler Fusion **55**, 023012 (2015).

[29]M.A. Chilenski, M.J. Greenwald, A.E. Hubbard, J.W. Hughes, J.P. Lee, Y.M. Marzouk, J.E. Rice, and A.E. White, Nucl. Fusion **57**, 126013 (2017).

[30]C.E. Rasmussen and C.K.I. Williams, *Gaussian Processes for Machine Learning* (Cambridge, MA: MIT Press) (2016).

[31]S. Watanabe, Journal of Machine Learning Research **11**, 3571 (2010).

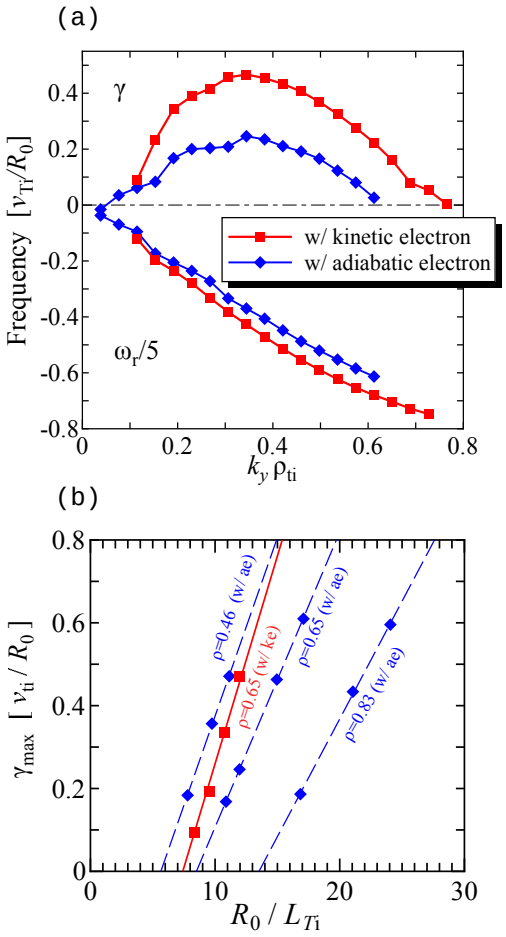

FIG. 1. (a) Poloidal wavenumber spectra of linear growth rates γ and real frequencies $\omega_{\rm r}$ of the micro-instabilities at $\rho = 0.65$, and (b) the ion temperature gradient dependences of $\gamma_{\rm max}$ obtained from the linear gyrokinetic simulations with kinetic electrons and the adiabatic electrons in the LHD high-$T_{\rm i}$ plasma. Red and blue symbols show the results in the simulations with kinetic electron model and the adiabatic electron model, respectively.

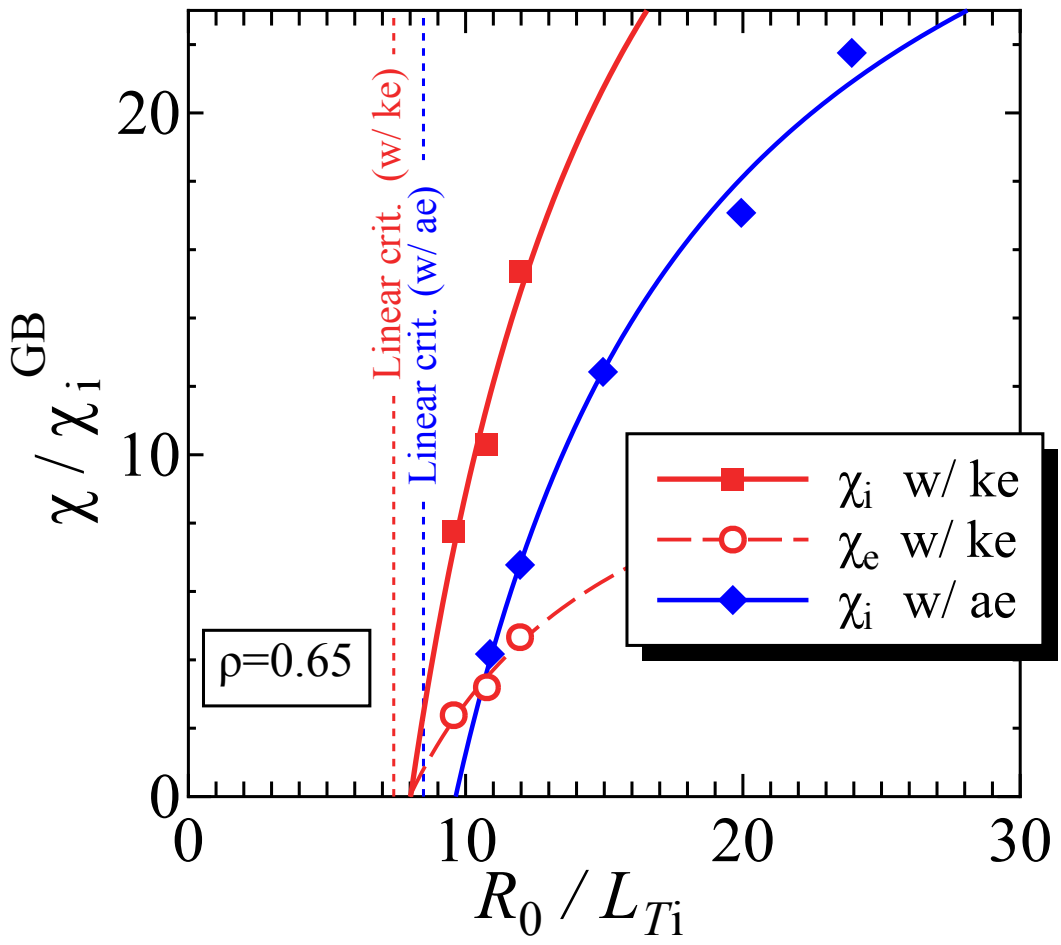

FIG. 2. The ion temperature gradient dependencies of the heat transport coefficients for ion (red squares) and electron (red circles) from electromagnetic gyrokinetic simulations with kinetic electrons at $\rho = 0.65$ in the LHD high-T_i plasma. Here, $\chi_\mathrm{i}^\mathrm{GB} = \rho_\mathrm{ti}^2 v_\mathrm{ti}/R_0$. Blue diamonds represent the ion heat transport coefficients from electrostatic simulations with adiabatic electrons. Dotted lines are the critical temperature gradients from linear analyses.

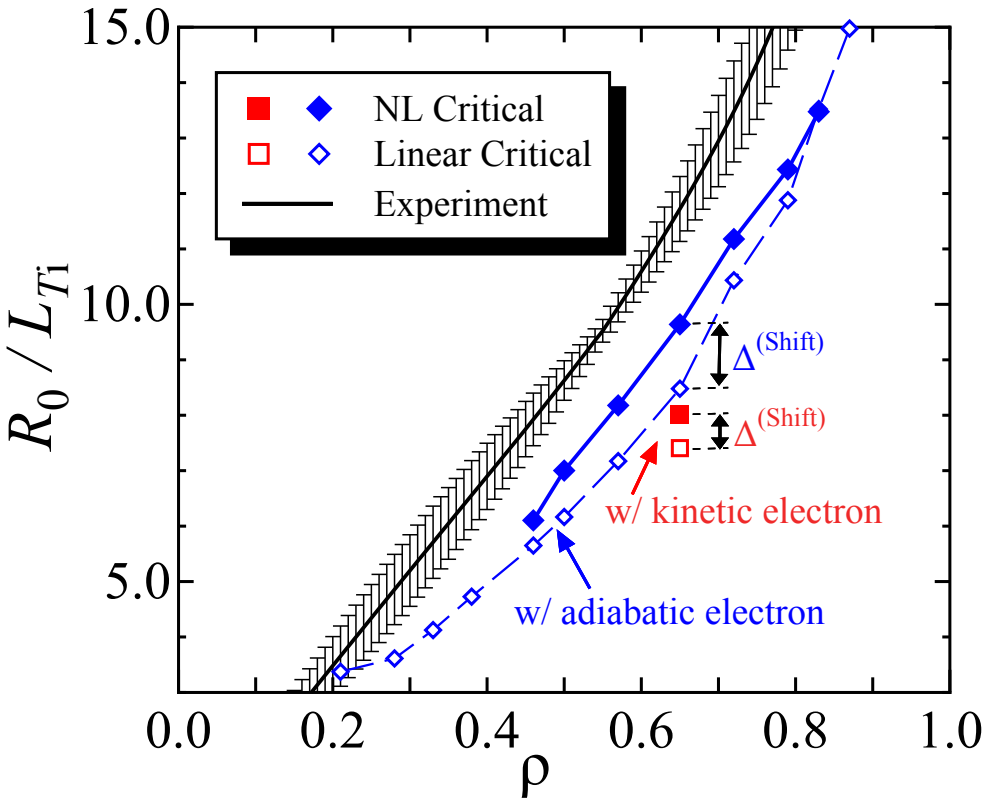

FIG. 3. Radial profile of the critical ion temperature gradient obtained from the simulation with kinetic electrons (red) and adiabatic electrons (blue). Filled symbols represent the nonlinear results and open symbols are linear results linear results, and $\Delta^{(\mathrm{shift})}$ correspond to Eq.(4). Black curve and errorbars show the radial gradients of the ion temperature from the experiment which will be discussed in Sec.IV.

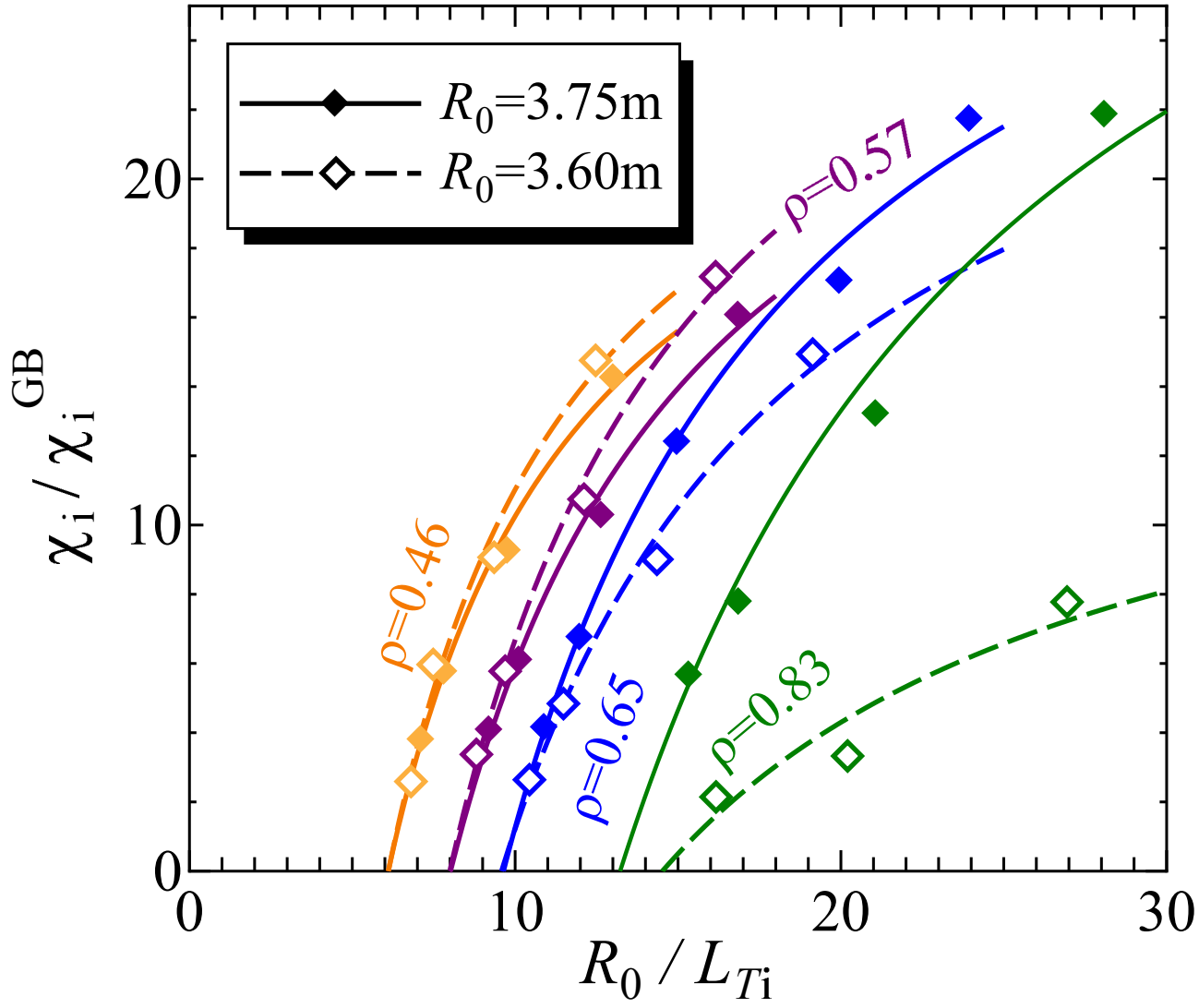

FIG. 4. The ion temperature gradient dependences of the ion heat transport coefficients at each radial position, $\rho = 0.46, 0.57, 0.65$ and 0.83 in the standard LHD case with $R_0 = 3.75$m (solid curves) and the inward shifted LHD case $R_0 = 3.6$m (dashed curves).

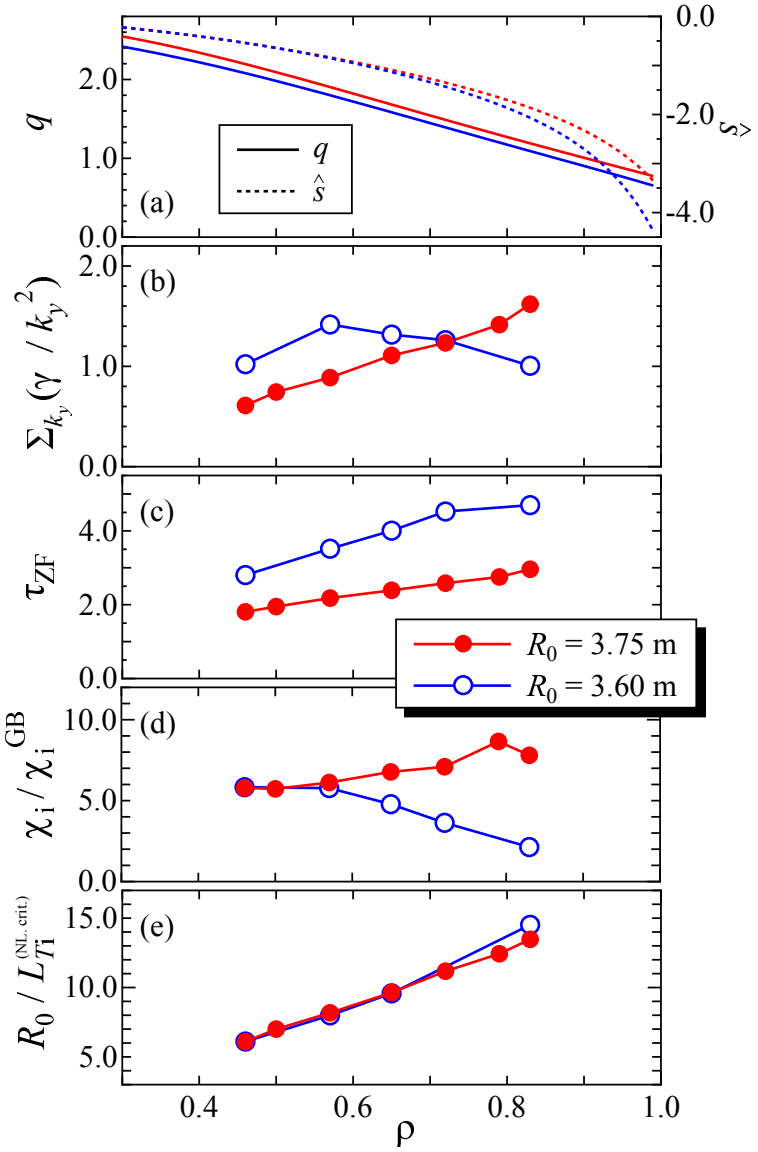

FIG. 5. Radial profiles of (a) the safety factor q and the magnetic shear $\hat{s}$, (b) the linear growth rates divided by the square of the poloidal wavenumber $\sum_{ky}(\gamma/k_y^2)$, (c) the zonal flow decay times $\tau_{\rm ZF}$, (d) the heat diffusivities, and (e) the nonlinear critical temperature gradients for the standard LHD case with $R_0 = 3.75$m (red solid curves) and the inward shifted LHD case with $R_0 = 3.6$m (blue dashed curves). In (b), (c), and (d) the results are obtained with the nominal ion temperature gradients.

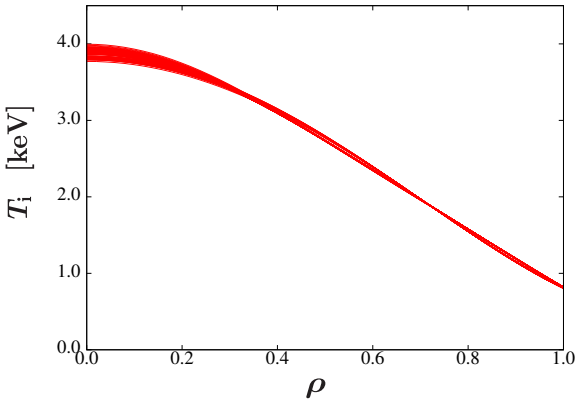

FIG. 6. The AIC results of the radial functions for the ion temperature.

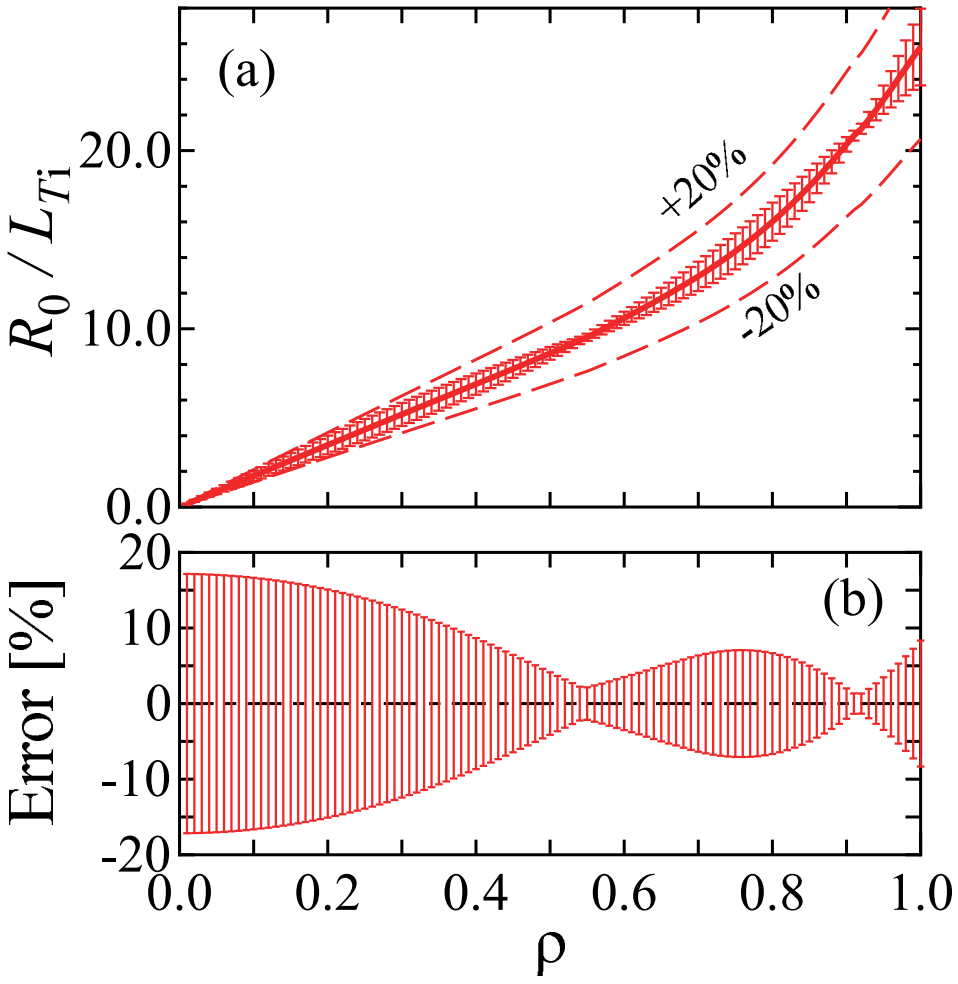

FIG. 7. The radial profile of (a) the radial gradients of the ion temperature with the ranges from the AIC theory, and (b) the relative error level of the ranges. In the top figure, ±20% of the medians of the temperature gradients are shown by the dashed curves.

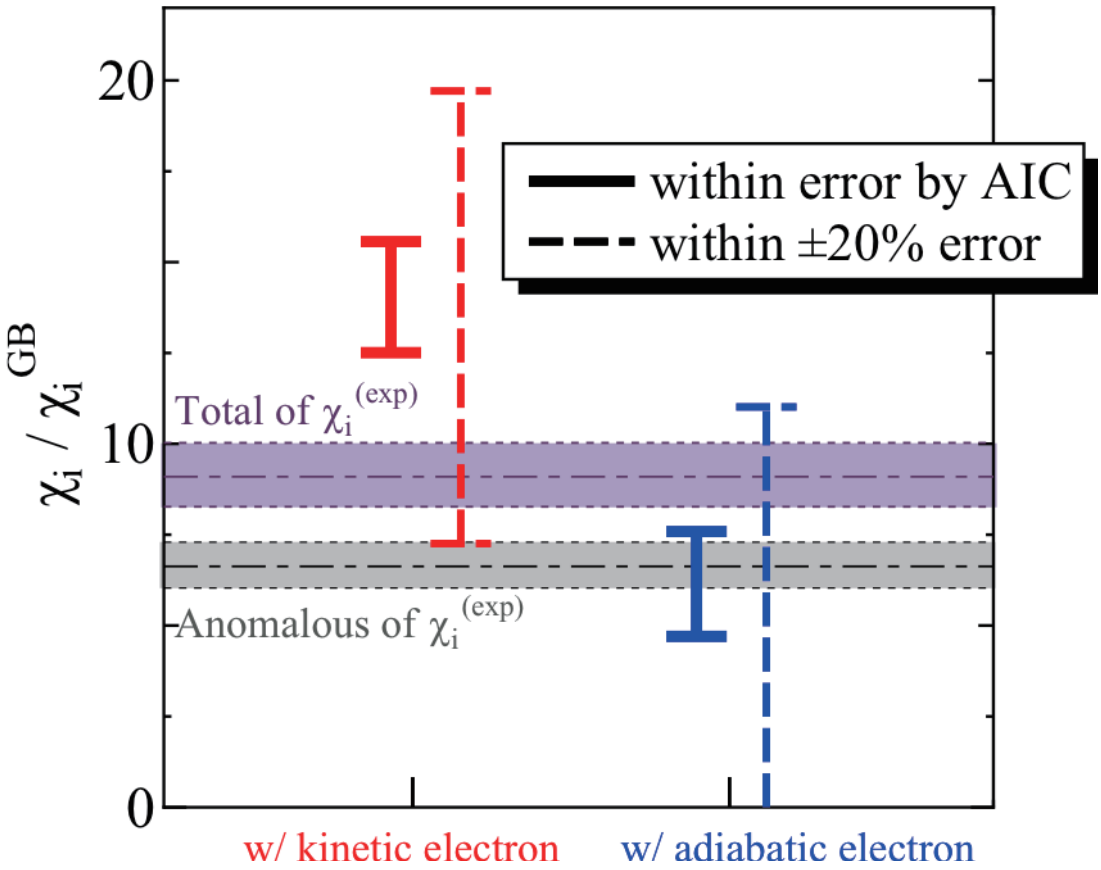

FIG. 8. The ranges of the ion heat transport coefficients at $\rho = 0.65$ obtained from the simulation with kinetic electrons (red) and the simulation with adiabatic electrons (blue) within the allowable ion temperature gradient range. Solid errorbars represent the ranges within the experimental errors of $R_0/L_{T\mathrm{i}}$ obtained by AIC technique and dashed errorbars show the ranges within ±20% of $R_0/L_{T\mathrm{i}}$. Hatched regions represent the total ion diffusivity (magenta) and the anomalous part of the diffusivity (gray) in the experiment.

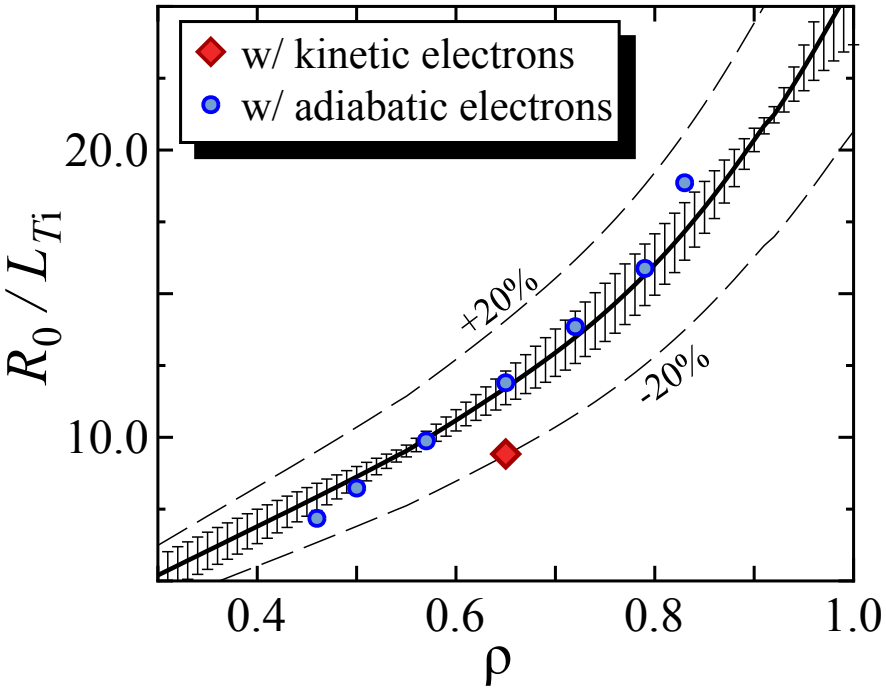

FIG. 9. Applications of the flux-matching method to expect the ion temperature gradients based on the simulations with kinetic electrons (red diamond) and with adiabatic electrons (blue circles). The allowable ranges of the temperature gradients from the experimental results evaluated by AIC theory are represented by the black curves and errorbars. Dashed curves represent ±20% of the nominal temperature gradients.